
Article:
Burman, Matthew and Noy, Agnes (2025) Atomic Description of the Reciprocal Action between Supercoils and Melting Bubbles on Linear DNA. Physical Review Letters. 038403. ISSN: 1079-7114

https://doi.org/10.1103/PhysRevLett.134.038403

Atomic Description of the Reciprocal Action between Supercoils and Melting Bubbles on Linear DNA

Matthew Burman and Agnes Noy*
School of Physics, Engineering and Technology, University of York, York YO10 5DD, United Kingdom

(Received 5 July 2023; accepted 18 December 2024; published 24 January 2025)

Although the mechanical response of DNA to physiological torsion and tension is well characterized, the detailed structures are not yet known. By using molecular dynamics simulations on linear DNA with 300 base-pairs, we provide, for the first time, the conformational phase diagram at atomic resolution. Our simulations also reveal the dynamics and diffusion of supercoils. We observe a new state in negative supercoiling, where denaturation bubbles form in adenine/thymine-rich regions independently of the underlying DNA topology. We thus propose sequence-dependent bubbles could position plectonemes in longer DNA.

DOI: 10.1103/PhysRevLett.134.038403

Inside living beings, DNA is subjected to torsional stress due to transcription and replication activity, as well as due to the wrapping around proteins such as gyrases [1], nucleosomes [2,3], or nucleoid-associated proteins [4]. This stress is relieved by the formation of intertwined loops (or plectonemes) and changes in molecular twist, promoting the formation of melting bubbles when the hydrogen bonds between base-pairs (bp) are disrupted. These structural changes are quantified by the linking number, $Lk = Tw + Wr$, where Tw (twist) is the number of times one strand revolves around the other in the double helix and Wr (writhe) is the number of times the DNA coils around itself. DNA supercoiling is one of the basic mechanisms that organizes genomes [5] and, due to its importance, is steadily controlled in cells at a superhelical density $\sigma = \Delta Lk/Lk_0 \approx -0.07$ [2,3,6], with Lk_0 being the default linking number in relaxed DNA.

At the same time, DNA is subjected to relatively small pulling forces due to routine activities like loop extrusion or molecular condensation (with < 1 pN) [7,8]. DNA nanomechanical properties have been studied *in vitro* by magnetic tweezers, which are able to impose both stretching and torsion upon a single molecule [9–12]. This experimental setup, together with the development of elastic rod models [13–15], created an initial picture of how the combination of these two forces disturbs DNA. At low stretching forces (F < 0.6 pN), the torsion is first absorbed by twist until it is energetically more favorable for

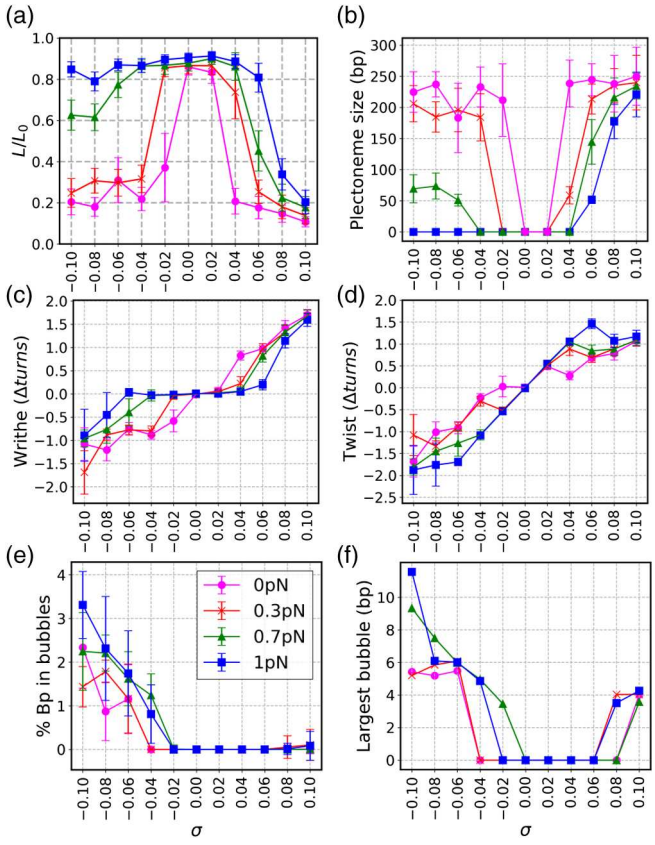

FIG. 1. Response of a 300-bp linear DNA molecule to torsion and tension in terms of relative extension L/L_0 (a), plectoneme size (b), writhe (c), twist (d), percentage of bp in bubbles (d), and size of the largest bubble (e). Values reported here are averages and standard deviations (error bars) over the last 400 ns of each all-atom simulation. Simulations at 0 pN are represented in pink with circles, at 0.3 pN in red with crosses, at 0.7 pN in green with triangles, and at 1 pN in blue with squares.

*Contact author: agnes.noy@york.ac.uk

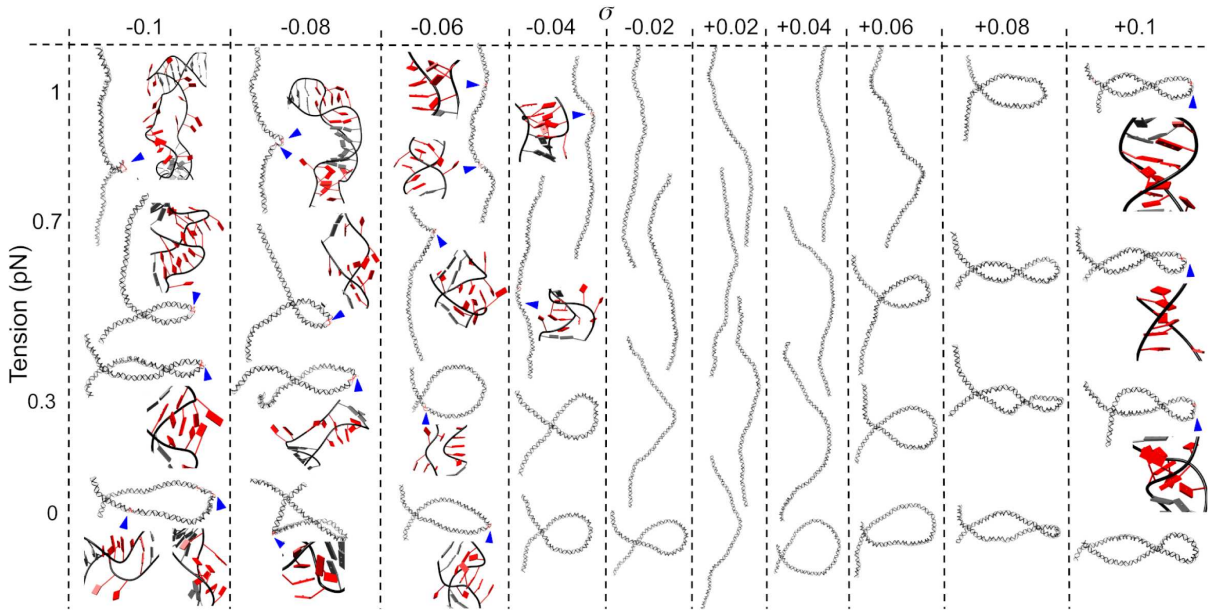

FIG. 2. A structural map of DNA under tension and torsion using a representative structure from each of our simulations, where bubbles are highlighted in red and signed by blue arrow heads, with most of them shown in detail by enlarged images. The structures inside each column are ordered from high (top) to low (bottom) tension. Those at $\sigma = 0$ have been excluded to facilitate visualization.

the molecule to buckle into a plectoneme, reducing DNA extension and absorbing torsion as writhe. At higher force values (F > 0.9 pN), DNA extension remains relatively constant at negative supercoiling due to the apparition of denaturation bubbles instead of plectonemes [16,17].

However, little is known about the actual configurations of DNA under these conditions because the molecule is not directly observable in this type of experiment. Previous coarse-grained simulations revealed that denaturation bubbles are placed at the tip of the plectonemes [18–20], instead of being completely independent of one another as was assumed before [10,11,14]. Cryotomography and atomic force microscopy were employed to visualize supercoiled DNA using minicircles of 300–400 bp and compare it to all-atom molecular dynamics (MD) simulations [21,22]. These studies detected the emergence of melting bubbles in the absence of tension, which suggests that the crosstalk between these and plectonemes might be more sophisticated than previously thought, opening the question as to their impact on linear DNA.

In this Letter, we report a comprehensive set of atomically precise MD simulations to investigate the interplay between supercoiled loops and melting bubbles on DNA under a physiological range of extension and supercoiling ($F = 0$, 0.3, 0.7, and 1 pN; $\sigma = 0$, ± 0.02, ± 0.04, ± 0.06, ± 0.08, and ± 0.1). To this end, we built linear DNA molecules of 300 bp in a perfectly straight conformation with different twist values for defining the various σ. The sequence was randomly generated containing an adenine/thymine (AT) percentage of 49%. DNA molecules were modeled using Amber18 [23], BSC1 force field [24], and the implicit generalized Born model [25–27] at a monovalent salt concentration of 0.2 M following our latest protocols [4,28] (see Supplemental Material [29] and Tables S1 and S2). To allow the redistribution of torsion into twist and writhe, we performed a 40-ns preliminary simulation stage with restraints on the bp hydrogen bonds to avoid premature breakage of the double helix [4] and restraints at the ends to maintain torsional stress (Fig. S1). In the production stage, the H-bond restraints were removed and a constant pulling force was applied (see Supplemental Material [29,30]). Simulations were extended to 0.5–2.7 μs depending on their convergence interval, which was monitored by the end-to-end distance over time (Figs. S2–S12). In total, we performed 44 different simulations giving a combined trajectory length of more than 32 μs. Only the last 400 ns of each simulation were used for subsequent analysis.

We measured twist and writhe using WrLINE [31] and DNA bending using SerraLINE [22]. Bend angles were calculated using a pair of tangent vectors, defined along the WrLINE molecular contour, separated by 16 nucleotides (approximately a helical turn and a half) as a compromise length for capturing the overall bend produced by a melting bubble or by canonical DNA (B-DNA). We determined the formation of melting bubbles by observing the interruption of 3 or more consecutive bp: canonical H bonds were all broken and angular bp parameters (propeller twist, opening, and buckle) were at least 2 standard deviations away from the average observed in relaxed DNA. The minimum time cutoff was set at 1 ns, as this is the approximate duration necessary for the bubble to significantly influence the global DNA conformation (Fig. S13). The size of supercoils was measured by projecting the trajectories onto

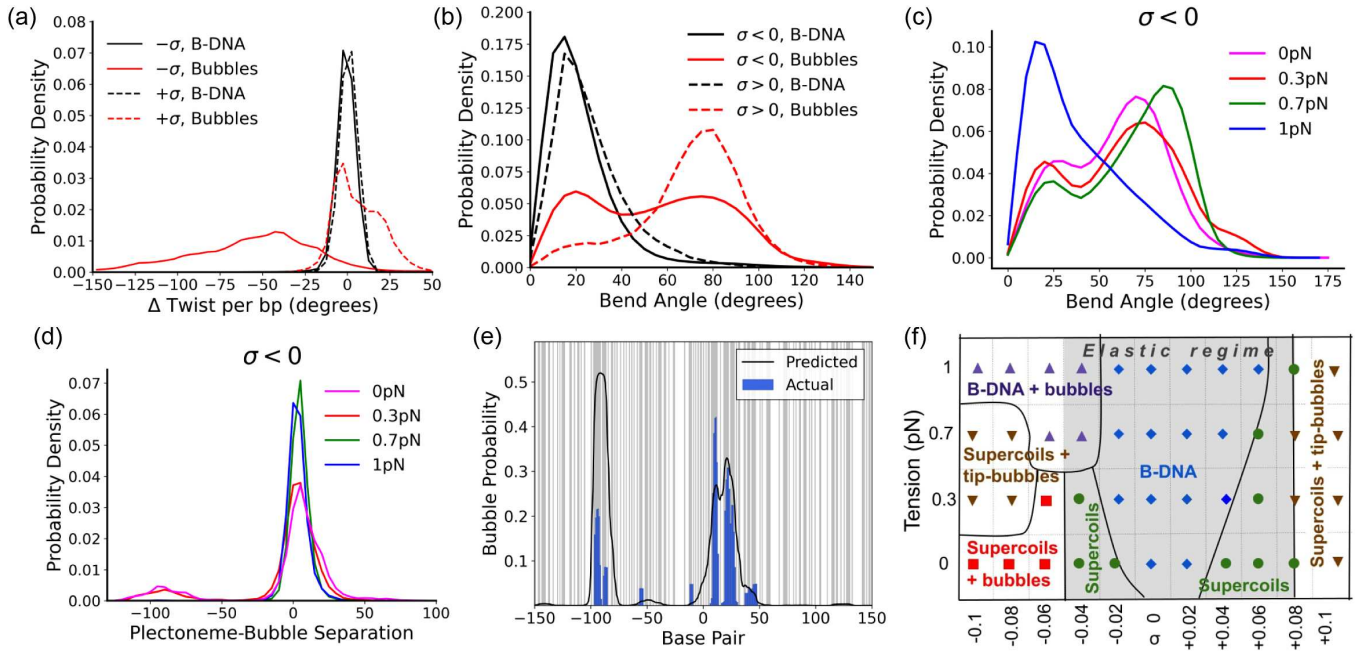

FIG. 3. DNA twist (a) and bend angle (b) across all simulations splitted by direction of supercoiling and underlying structure. (c) DNA bend angle of denaturation bubbles formed under negative supercoiling as a function of tension. (d) Distance between the centers of plectonemes and bubbles for negatively supercoiled DNA as a function of tension. (e) Position of denaturation bubbles predicted by the SIDD model (black) and observed in our negative supercoiling simulations (blue). A:T bp are shaded in gray. (f) Phase diagram summarizing the simulation results showing the various conformational states: extended B-DNA (blue diamonds), B-DNA and bubbles (purple triangles), supercoils (green circles), supercoils and bubbles (red squares), and supercoils with tip-bubbles (inverted brown diamonds). The area where DNA follows the elastic regime is shaded in gray.

the best-fit plane using SerraLINE and by detecting crossing points formed by two bp placed < 3 Å to each other and at least 40 bp apart along the molecular contour.

Overall, our simulations show good agreement with experimental "hat curves" [10–12] (Figs. 1 and S14, and Table S3). They are able to reproduce the reduction of DNA end-to-end distance at low forces, its flattening at 1 pN for $\sigma < 0$, as well as the transition between extended and plectonemic states at the critical tension of 0.7 pN.

For moderate levels of supercoiling ($-0.04 \leq \sigma \leq +0.06$), DNA follows the predictions of simple elastic rod models, where chiral loops and bubbles are excluded from each other (Figs. 1, 2, and S2–S12). We observe a separation between twist-dominated and writhe-dominated states: as $|\sigma|$ increases, the buckling transition occurs [Figs. 1(a) and 1(b)], inducing writhe [Fig. 1(c)] while maintaining twist levels similar to those in relaxed DNA or in lower torsional stress [Fig. 1(d)]. When DNA is extended, the torsional stress is accommodated by changes in the molecular twist until the canonical hydrogen bonds and stacking interactions begin to break, resulting in the formation of melting bubbles [Fig. 1(e) and Video S1]. Then, these bubbles act as flexible torsional spots that can incorporate the excess of superhelical stress (Fig. 3) [32,33]. In addition, we observe that simulations with intermediate end-to-end distances (e.g., $\sigma = -0.02$ at 0 pN and $\sigma = 0.04$ at 0.3 pN) present large fluctuations due to the oscillations between the extended and the buckled phases, as was seen before [34,35] [see Figs. 1(a) and S15 and Videos S2, S3, and S4].

At low σ values, buckled DNA consists of single chiral loops (Fig. 2), which resemble the "curls" predicted by the elastic theory that appear before the extrusion of plectonemes [36–38] and can diffuse over short distances (Fig. 4 and Video S4). When enough torsional stress is imposed ($|\sigma| \geq 0.08$), our modeled DNA presents proper plectonemes (with more than one crossing point) of 8 ± 1 nm of diameter. These structures are similar to those observed on DNA minicircles [22], suggesting that their behavior is representative of that observed in linear DNA. In general, we observe that plectonemes tend to occupy the entire length, so they are pinned in the middle of our DNA sequence [Figs. 1(b) and 2].

DNA under highly negative supercoiling ($\sigma \leq -0.06$) presents most of the melting bubbles at the tip of plectonemes [Figs. 3(d) and S5–S7], because the high curvature there promotes the disruption of the double helix [18,22]. In addition, the high flexibility of melting bubbles accommodates further sharp bends [Fig. 3(b)], allowing the compaction of plectonemes and thus an increase of end-to-end distances under tension [18]. In agreement with these predictions, we observe plectoneme tip-bubbles to be especially prominent at the critical tension of 0.7 pN (Figs. 2 and 3). Moreover, these "tip-bubbles" are expected

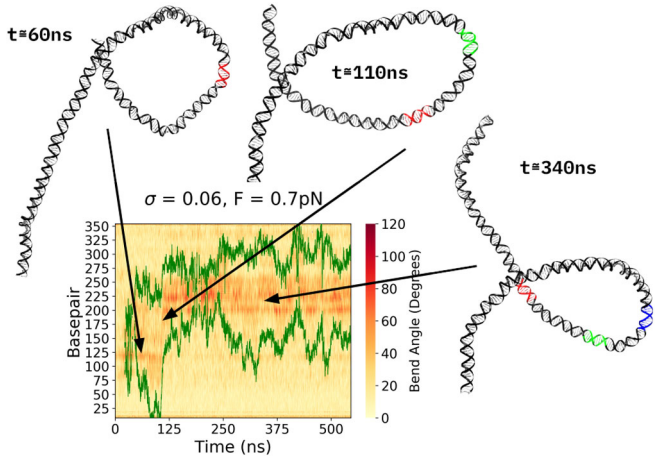

FIG. 4. Migration of the supercoiled loop from the simulation at $\sigma = 0.06$ and 0.7 pN. The kymograph shows loop's start and end points as green lines and DNA local bends as background heatmap. Representative structures show the DNA parts that are sequentially positioned at the tip of the loop: in red at 60 ns, in green at 110 ns, and in blue at 340 ns.

to grow when tension is raised, causing shrinking and eventually vanishing of plectonemes [18], as we can see in our simulation at $\sigma = -0.1$ and 1 pN (Fig. S7 and Video S5). We also observe that the size of the largest bubbles for $\sigma = -0.1$ increases from ~5 bp in 0–0.3 pN to 11 bp in 1 pN [Fig. 1(e)].

However, our all-atom simulations indicate more complex behavior than expected, due to the development of bubbles induced by negative supercoiling rather than tension. This is consistent with previous experiments that detected melting bubbles in circular DNA of 650–700 bp due to their susceptibility to Bal-31, a nuclease that cleaves single-stranded DNA [39]. At 0 pN, we observe the presence of multiple bubbles in the arms of plectonemes, which can present the same degree of bending as B-DNA [Figs. 2 and 3(b) and Video S6]. Then, for our simulations at $\sigma \leq -0.08$, the introduction of pulling tension promotes the concentration of denaturation into a single bubble at the tip of plectonemes, thus converging into the insights given by the oxDNA model [18] [Figs. 2 and 3(d)]. At $\sigma = -0.06$, which is close to the targeted supercoiling level of living organisms [2,3,6], we observe an intermediate behavior between high and low supercoiling regimes: bubbles appear irrespective of tension and tip-bubbles are not needed for the transition into the extended state (Figs. 2 and S5 and Video S7). In summary, we show that the DNA structural response for $\sigma \leq -0.06$ is highly convoluted as torsional stress can be simultaneously dissipated via plectonemes, or writhe [Figs. 1(b) and 1(c)], and melting bubbles, or twist [Figs. 1(d) and 1(e)].

To confirm the formation of melting bubbles in the absence of tension, we conducted simulations in explicit solvent following our standard protocols [28] (see Supplemental Material [29], which includes [40–44]).

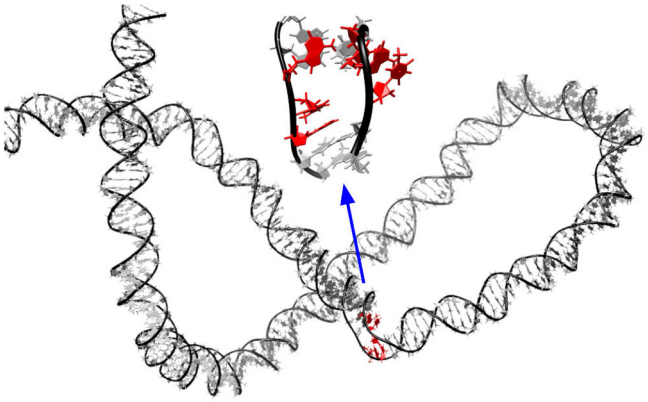

FIG. 5. Representative frame from the explicitly solvated simulation at $\sigma = -0.06$ and zero tension presenting a melting bubble in one of the plectoneme's arms (in red and enlarged).

The starting structures for these simulations were derived from the preliminary phase of the above implicit solvent simulations. They were performed with both DNA ends locked to preserve torsional stress and without pulling force. Despite the short simulation time (100 ns) due to the system's large size, a melting bubble emerged in one of the plectoneme's arms at $\sigma = -0.06$ lasting more than 40 ns (Figs. 5 and S16 and Video S8). Simulations with $\sigma \leq -0.08$ resulted in long-lived double-helix disruptions such as kinks and 2-bp bubbles, while little to no helical disruption was observed at $\sigma = -0.04$ (Figs. S16 and S17).

An additional consequence of tension-independent bubbles in negative supercoiling is that their positioning not only depends on the location of plectonemes but also on DNA sequence. As predicted by the SIDD (stress-induced DNA destabilization) program [45], our molecule presents two spots particularly prone to denature due to their high AT content: the first one is close to the center and strongly aligns with the tip of plectonemes; the second one is located ~85 bp off-center and coincides with a small peak of denaturation [see Fig. 3(e)]. Interestingly, while this second site is minor in our simulations, it has the highest probability according to the SIDD model. This model is based purely on thermal denaturation energies and therefore fails to account for the effects of DNA curvature [45]. Hence, our results indicate that, in short DNAs, the location of melting bubbles is balanced between the presence of AT-rich sequences and the location of the tip of the plectoneme, which is forced to be in the middle. For longer DNAs, where several plectonemes can coexist [36,46], we anticipate a different scenario: melting bubbles could nucleate the extrusion of plectonemes, making SIDD predictions valid for the location of the latter as well as the former [47].

Our simulations show that highly positive supercoiled DNA ($\sigma \geq +0.08$) can present denaturation bubbles, even in the absence of tension, in agreement with recent biochemical experiments on DNA minicircles [39] (see Figs. 1 and 2). In contrast to negative supercoiling, these

melting bubbles are smaller, less stable, and always placed near the tip of plectonemes (Figs. 2, S11, and S12 and Video S9). Because these bubbles are less efficient than those in unwound DNA at incorporating excess twist [Fig. 3(a)], they cannot follow the same mechanism: they cannot grow under tension to eventually substitute the plectonemic loop. Nevertheless, they still bring additional assimilation of superhelical stress in the form of writhe: the accommodation of a strong bend at the tip of plectonemes enables loop tightening, thus allowing further coiling on DNA [Figs. 1–3(b)]. These bubbles can also present moderate bends in the range of B-DNA when they slightly move from the tip of the plectoneme [Figs. 3(b) and S18 and Video S9]. In general, our simulations show that, in this high positive supercoiling regime, melting bubbles are always nucleated after the formation of plectonemes because they are promoted by high curvature. Hence, our study supports the model deduced by Dekker and co-workers, in which the position of plectonemes is controlled by the curvature of B-DNA [48].

Conclusions—Our simulations successfully connect extension-rotation curves obtained by magnetic tweezers with microscopy and biochemical data from circular DNA demonstrating that the structural features observed in the latter are also present in linear DNA. Hence, we can provide, for the first time, a phase diagram of the DNA conformation at atomic resolution under physiological levels of torsion and tension [Fig. 3(f)]. The elastic regime, where supercoils and bubbles are excluded from each other, is mapped at $-0.04 \leq \sigma \leq +0.06$ and the plectoneme tip-bubbles described by coarse-grained simulations are at $\sigma \leq -0.08$ and 0.3–0.7 pN. In addition, we uncover two new conformational states: plectoneme tip-bubbles for $\sigma \geq +0.08$ and melting bubbles nucleated in AT-rich regions for $\sigma \leq -0.06$ and minimal tension. Although the boundaries between the main states may slightly shift when considering other sequences and ion conditions, we expect that their overall distribution across the tension-torsion phase diagram will remain unchanged. At the length of our modeled DNA (300 bp), sequence-dependent bubbles are not necessarily placed at the tip, as this is constrained to be in the middle. However, for longer DNA, where plectonemes have room for relocating, sequence-dependent bubbles could have a key role in nucleating them. We anticipate that these states will be important for the regulation of loops in promoters (with size 100–1000 bp [49]) and of larger topological domains.

Acknowledgments—This work was supported by EPSRC: EP/N027639/1 (A. N.) and EP/R513386/1 (M. B.), as well as EP/T022205/1, EP/X035603/1, EP/P020259/1, and EP/T022167/1 (computational resources).

Data availability—Simulations are available at [50]. We thank D. Salerno and J. van Noort for sharing their data.

[1] M. Vayssières, N. Marechal, L. Yun, B. L. Duran, N. K. Murugasamy, J. M. Fogg, L. Zechiedrich, M. Nadal, and V. Lamour, Science **384**, 227 (2024).
[2] A. Bancaud, N. Conde e Silva, M. Barbi, G. Wagner, J.-F. Allemand, J. Mozziconacci, C. Lavelle, V. Croquette, J.-M. Victor, A. Prunell, and J.-L. Viovy, Nat. Struct. Mol. Biol. **13**, 444 (2006).
[3] A. Kaczmarczyk, H. Meng, O. Ordu, J. Noort, and N. H. Dekker, Nat. Commun. **11**, 126 (2020).
[4] G. D. Watson, E. W. Chan, M. C. Leake, and A. Noy, Comput. Struct. Biotech. J. **20**, 5264 (2022).
[5] S. Martis B., R. Forquet, S. Reverchon, W. Nasser, and S. Meyer, Comput. Struct. Biotech. J. **17**, 1047 (2019).
[6] E. Zechiedrich, A. B. Khodursky, S. Bachellier, R. Schneider, D. Chen, D. M. Lilley, and N. R. Cozzarelli, J. Biol. Chem. **275**, 8103 (2000).
[7] S. Golfier, T. Quail, H. Kimura, and J. Brugués, eLife **9**, e53885 (2020).
[8] T. Quail, S. Golfier, M. Elsner, K. Ishihara, V. Murugesan, R. Renger, F. Jülicher, and J. Brugués, Nat. Phys. **17**, 1007 (2021).
[9] T. R. Strick, J. F. Allemand, D. Bensimon, A. Bensimon, and V. Croquette, Science **271**, 1835 (1996).
[10] D. Salerno, A. Tempestini, I. Mai, D. Brogioli, R. Ziano, V. Cassina, and F. Mantegazza, Phys. Rev. Lett. **109**, 118303 (2012).
[11] H. Meng, J. Bosman, T. van der Heijden, and J. van Noort, Biophys. J. **106**, 1174 (2014).
[12] R. Vlijm, J. v. d. Torre, and C. Dekker, PLoS One **10**, e0141576 (2015).
[13] J. F. Marko and E. D. Siggia, Phys. Rev. E **52**, 2912 (1995).
[14] J. F. Marko, Phys. Rev. E **76**, 021926 (2007).
[15] N. Clauvelin, B. Audoly, and S. Neukirch, Macromolecules **41**, 4479 (2008).
[16] J. F. Allemand, D. Bensimon, R. Lavery, and V. Croquette, Proc. Natl. Acad. Sci. U.S.A. **95**, 14152 (1998).
[17] T. R. Strick, V. Croquette, and D. Bensimon, Proc. Natl. Acad. Sci. U.S.A. **95**, 10579 (1998).
[18] C. Matek, T. E. Ouldridge, J. P. K. Doye, and A. A. Louis, Sci. Rep. **5**, 7655 (2015).
[19] P. R. Desai, S. Brahmachari, J. F. Marko, S. Das, and K. C. Neuman, Nucleic Acids Res. **48**, 10713 (2020).
[20] W. Lim, F. Randisi, J. P. K. Doye, and A. A. Louis, Nucleic Acids Res. **50**, 2480 (2022).
[21] R. N. Irobalieva, J. M. Fogg, D. J. Catanese, T. Sutthibutpong, M. Chen, A. K. Barker, S. J. Ludtke, S. A. Harris, M. F. Schmid, W. Chiu, and L. Zechiedrich, Nat. Commun. **6**, 8440 (2015).
[22] A. L. B. Pyne, A. Noy, K. H. S. Main, V. Velasco-Berrelleza, M. M. Piperakis, L. A. Mitchenall, F. M. Cugliandolo, J. G. Beton, C. E. M. Stevenson, B. W. Hoogenboom, A. D. Bates, A. Maxwell, and S. A. Harris, Nat. Commun. **12**, 1053 (2021).
[23] D. A. Case *et al.*, *AMBER* (2018), Vol. 18.
[24] I. Ivani, P. D. Dans, A. Noy, A. Pérez, I. Faustino, A. Hospital, J. Walther, P. Andrio, R. Goñi, A. Balaceanu, G. Portella, F. Battistini, J. L. Gelpí, C. González, M. Vendruscolo, C. A. Laughton, S. A. Harris, D. A. Case, and M. Orozco, Nat. Methods **13**, 55 (2015).

[25] A. Perez, J. L. MacCallum, E. Brini, C. Simmerling, and K. A. Dill, J. Chem. Theory Comput. **11**, 4770 (2015).
[26] H. Nguyen, A. Pérez, S. Bermeo, and C. Simmerling, J. Chem. Theory Comput. **11**, 3714 (2015).
[27] R. Anandakrishnan, A. Drozdetski, R. C. Walker, and A. V. Onufriev, Biophys. J. **108**, 1153 (2015).
[28] S. Yoshua, G. Watson, J. A. L. Howard, V. Velasco-Berrelleza, M. Leake, and A. Noy, Nucleic Acids Res. **49**, 8684 (2021).
[29] See Supplemental Material at http://link.aps.org/supplemental/10.1103/PhysRevLett.134.038403 for additional details on methods, videos, structures, kymographs, and comparison with experimental data.
[30] N. M. Henriksen, A. T. Fenley, and M. K. Gilson, J. Chem. Theory Comput. **11**, 4377 (2015).
[31] T. Sutthibutpong, S. A. Harris, and A. Noy, J. Chem. Theory Comput. **11**, 2768 (2015).
[32] T. Sutthibutpong, C. Matek, C. Benham, G. G. Slade, A. Noy, C. Laughton, J. P. Doye, A. A. Louis, and S. A. Harris, Nucleic Acids Res. **44**, 9121 (2016).
[33] K. Liebl and M. Zacharias, PLoS One **15**, e0232976 (2020).
[34] E. Skoruppa and E. Carlon, Phys. Rev. E **106**, 024412 (2022).
[35] W. Vanderlinden, E. Skoruppa, P. J. Kolbeck, E. Carlon, and J. Lipfert, Proc. Natl. Acad. Sci. Nexus **1**, pgac268 (2022).
[36] J. F. Marko and S. Neukirch, Phys. Rev. E **85**, 011908 (2012).
[37] A. Dittmore, J. Silver, and K. C. Neuman, J. Phys. Chem. B **122**, 11561 (2018).
[38] K. Ott, L. Martini, J. Lipfert, and U. Gerland, Biophys. J. **118**, 1690 (2020).
[39] J. M. Fogg, A. K. Judge, E. Stricker, H. L. Chan, and L. Zechiedrich, Nat. Commun. **12**, 5683 (2021).
[40] D. E. Smith and L. X. Dang, J. Chem. Phys. **100**, 3757 (1994).
[41] H. J. C. Berendsen, J. P. M. Postma, W. F. van Gunsteren, A. DiNola, and J. R. Haak, J. Chem. Phys. **81**, 3684 (1984).
[42] T. Darden, D. York, and L. Pedersen, J. Chem. Phys. **98**, 10089 (1993).
[43] J. P. Ryckaert, G. Ciccotti, and H. J. C. Berendsen, J. Comput. Phys. **23**, 327 (1977).
[44] V. Velasco-Berrelleza, M. Burman, J. W. Shepherd, M. C. Leake, R. Golestanian, and A. Noy, Phys. Chem. Chem. Phys. **22**, 19254 (2020).
[45] C. J. Benham and C. Bi, J. Comput. Biol. **11**, 519 (2005).
[46] M. T. J. van Loenhout, M. V. de Grunt, and C. Dekker, Science **338**, 94 (2012).
[47] J. W. Shepherd, S. Guilbaud, Z. Zhou, J. A. L. Howard, M. Burman, C. Schaefer, A. Kerrigan, C. Steele-King, A. Noy, and M. C. Leake, Nat. Commun. **15**, 2748 (2024).
[48] S. H. Kim, M. Ganji, E. Kim, J. van der Torre, E. Abbondanzieri, and C. Dekker, eLife **7**, e36557 (2018).
[49] E. Kristiansson, M. Thorsen, M. J. Tamás, and O. Nerman, Mol. Biol. Evol. **26**, 1299 (2009).
[50] University of York Data Repository, 2024, 10.15124/6e19b09d-04cd-4472-b448-e4e18d2a6024.